

Physical characterization of double asteroid (617) Patroclus from 2007/2012 mutual events observations

J. Berthier^a, P. Descamps^{a,*}, F. Vachier^a, J. Normand^a, L. Maquet^a, F. Deleflie^a, F. Colas^a, A. Klotz^b, J.-P. Teng-Chuen-Yu^c, A. Peyrot^c, F. Braga-Ribas^{d,e,f}, F. Marchis^g, A. Leroy^h, S. Bouley^h, G. Dubos^h, J. Pollockⁱ, T. Pauwels^j, P. Vingerhoets^j, J.A. Farrell^k, P.V. Sada^l, V. Reddy^m, K. Archerⁿ, H.H. Hamanowa^o

^a Institut de Mécanique Céleste et de Calcul des Éphémérides, Observatoire de Paris, UMR8028 CNRS, 77 av. Denfert-Rochereau, 75014 Paris, France

^b Institut de Recherche en Astrophysique et Planétologie, 9, avenue du Colonel Roche, 31028 Toulouse, France

^c Observatoire des Makes, 18, rue G. Bizet - Les Makes, 97421 La Rivière, France

^d Federal University of Technology - Paraná (UTFPR / DAFIS), Rua Sete de Setembro, 3165, Curitiba (PR), Brazil

^e Observatório Nacional/MCTIC, R. General José Cristino 77, Bairro Imperial de São Cristóvão, Rio de Janeiro (RJ), Brazil

^f Laboratório Interinstitucional de e-Astronomia - LIneA & INCT do e-Universo, Rua Gal. José Cristino 77, Bairro Imperial de São Cristóvão, Rio de Janeiro (RJ), Brazil

^g SETI Institute, Carl Sagan Center, 189 Bernardo Avenue, Mountain View, CA 94043, USA

^h Association T60, Observatoire Midi-Pyrénées, 14 avenue Edouard Belin, 31400 Toulouse, France

ⁱ Physics and Astronomy Department, Appalachian State University, Boone, NC 28608, USA

^j Royal Observatory of Belgium, Ringlaan 3, B-1180 Brussel, Belgium

^k Sulphur Flats Observatory, 449 Sulphur Creek Road, Jemez Springs, NM 87025, USA

^l Departamento de Física y Matemáticas, Universidad de Monterrey, Av. I. Morones Prieto 4500 Pte, San Pedro Garza García, N.L 66238, Mexico

^m Lunar and Planetary Laboratory, University of Arizona, 1629 East University Boulevard, Tucson, AZ 85721, USA

ⁿ Ironwood Observatory, HI, USA

^o Hamanowa Astronomical Observatory, Fukushima, Japan

ARTICLE INFO

Keywords:

Asteroids
Rotation
Surfaces - satellites of asteroids - eclipses - photometry

ABSTRACT

We publish a set of 16 light curves of mutual events inside the synchronous system of the Jupiter Trojan (617) Patroclus. Patroclus is the only binary system of the six target asteroids of the forthcoming NASA Discovery-class mission *Lucy*. Determining the physical parameters of the system is therefore of primary importance in helping to plan the flyby mission.

Light curves were acquired during two follow-up campaigns of 6 months each between January–June 2007 and July–December 2012. Eight small eclipse events of amplitude of 0.2–0.3 mag were recorded in 2007. On the other hand, in 2012, the amplitudes of the phenomena were much deeper, between 0.6 and 0.8 mag, due to a nearly edge-on configuration of the system.

We refined the sidereal period to $102.78624 \pm 0.00015h = 4.282760 \pm 0.000005$ days. The J2000 ecliptic coordinates of the pole of the system were found to be $\lambda = 235.3 \pm 1.2^\circ$ and $\beta = -62.4 \pm 0.2^\circ$. The volume ratio was determined equal to $q = 0.69 \pm 0.08$. By using a model of inhomogeneous Roche ellipsoids in hydrostatic equilibrium, we derived a bulk density of $0.81 \pm 0.16g/cm^3$ and a surface grain density of $2.69 \pm 0.36g/cm^3$ in agreement with spectroscopic observations of this P-type asteroid.

As a validation, our solution was applied to revisit recent results obtained from observations of another type: AO astrometry and stellar occultation. Our model is thus perfectly able to account for these observations after fitting the mutual separation to the value of 695 ± 10 km. Consequently, the area-equivalent diameter of the system as a whole is derived $D_A = 168.8 \pm 2.6$ km.

* Corresponding author at: IMCCE, Paris Observatory, 77, avenue Denfert-Rochereau, 75014 Paris, France.

E-mail address: descamps@imcce.fr (P. Descamps).

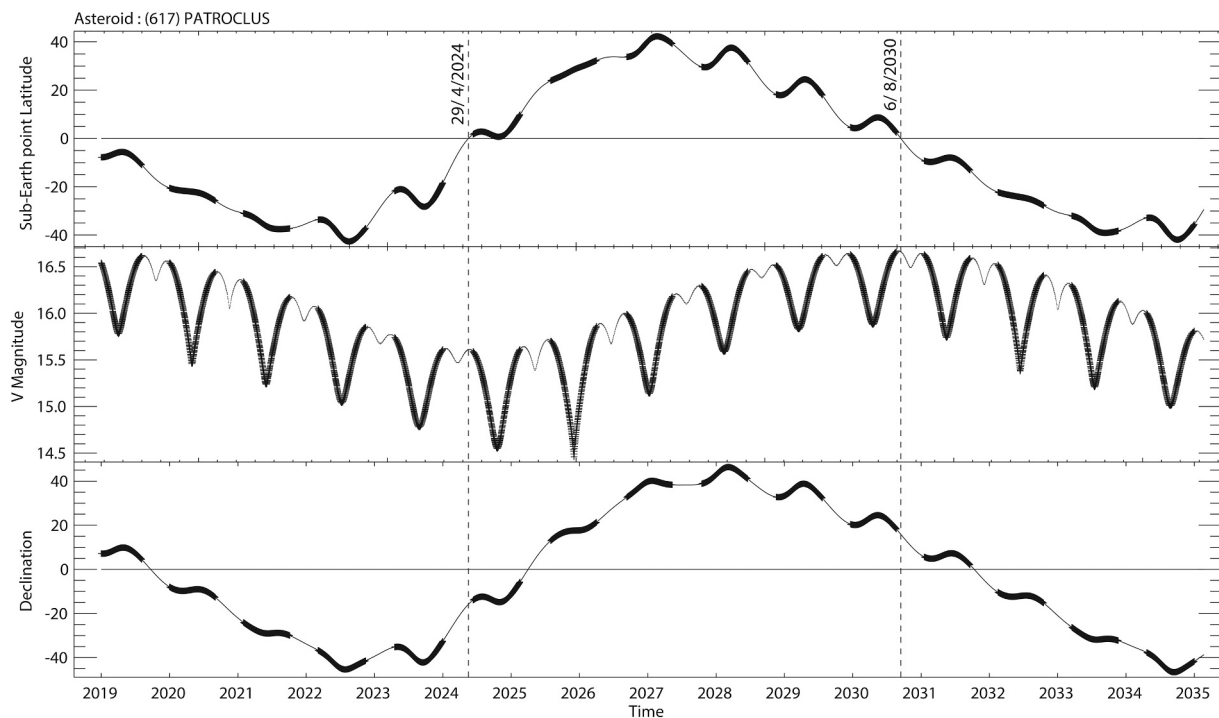


Fig. 1. Sub-solar latitude, V magnitude and declination of Patroclus versus time. The bold curves give the epochs where Patroclus is observable when the solar elongation is greater than 60°. The vertical line indicates when the system is perfectly viewed edge-on. Next mutual event seasons will occur from April 2024 to December 2024 and January 2030 to June 2030. Oppositions are given by the minima of the V magnitude curve.

Table 1
List of the observers with their facilities.

Observers	Observatory	IAU code	Aperture (m)	Campaign
F. Vachier, A. Klotz, F. Colas, F. Deleflie, L. Maquet, J. Normand, P. Descamps	Observatoire des Makes, Ile de la Réunion, France	181	0.6	2012
F. Vachier, F. Colas	Station de Planétologie des Pyrénées, Pic du Midi de Bigorres, France	586	1.0	2007, 2012
F. Braga Ribas, F. Vachier	Zeiss telescope of the Laboratório Nacional de Astrofísica (LNA), Itajubá, Brazil	874	0.6	2012
A. Leroy, S. Bouley, G. Dubos	Pic du Midi de Bigorres, France	586	0.6	2007
J. Pollock	PROMPT, Cerro Tololo Inter-American Observatory, Chile	807	0.41	2007
T. Pauwels, P. Vingerhoets	Royal Observatory of Belgium, Uccle, Belgium	012	1.2	2007
P. Descamps, F. Vachier	Observatoire de Haute Provence, France	511	1.2	2007
J. A. Farrell	Sulphur Flats Observatory, La Cueva, USA	H02	0.41	2007
P. V. Sada	Universidad de Monterrey, Mexico	720	0.35	2007
V. Reddy, K. Archer	Badlands Observatory, USA	918	0.66	2007
H. & H. Hamanowa	Hamanowa Astronomical Observatory, Japan	D91	0.4	2007
F. Marchis, V. Reddy	Lick Observatory, USA	662	1.0	2007

1. Introduction

The Trojan minor planet (617) Patroclus was found to be binary with components of similar size by direct imaging by Merline et al. (2001). It was the first known binary Jupiter Trojan. Since that time, the Patroclus system has been scrutinized with different instruments, mainly in adaptive optics, to study its physical and dynamical properties (Marchis et al., 2006a, 2006b, 2010, Buie et al., 2015, Grundy et al., 2018, Wong and Brown, 2019). From the first report of a single-periodic lightcurve with a full complete rotational coverage, the system was definitely characterized as fully synchronized with rotational period of each component equal to the period of the mutual orbit (Mueller et al., 2010).

Patroclus is one of the five Trojan flyby targets of the forthcoming NASA Discovery-class mission Lucy scheduled in 2021 with encounters from 2025 to 2033 (Levison and Lucy Science Team, 2016).

A precise determination of the orbit period, orbit plane and pole position that will result from observations of mutual events is essential for planning the Lucy mission’s encounter with this system.

In 2007 and 2012, the Earth crossed the orbital plane of the components of Patroclus system. Patroclus and Menoetius take turns eclipsing or occulting one another. We took this opportunity to collect photometric observations of mutual events inside the Patroclus-Menoetius system. In particular, we tried to target the periods of time where mutual phenomena (eclipses and occultations between the system components) occur. Two international campaigns were organized in 2007 (Berthier et al., 2007) and 2012. As for the 2018–2019 phenomena, only one event was reported to date (Wong and Brown, 2019). The next mutual event season will occur during April–December 2024 (Fig. 1). Such phenomena are essential for constraining the main dynamical and physical parameters of the system, namely, the period of rotation, the position of the pole of rotation in space, the relative shapes and sizes of the components, and their relative orbital motion by application of Kepler’s laws. The most fundamental physical parameter that can then be deduced is the bulk density. However, if a certain level of internal inhomogeneity is taken into account, it is also possible to

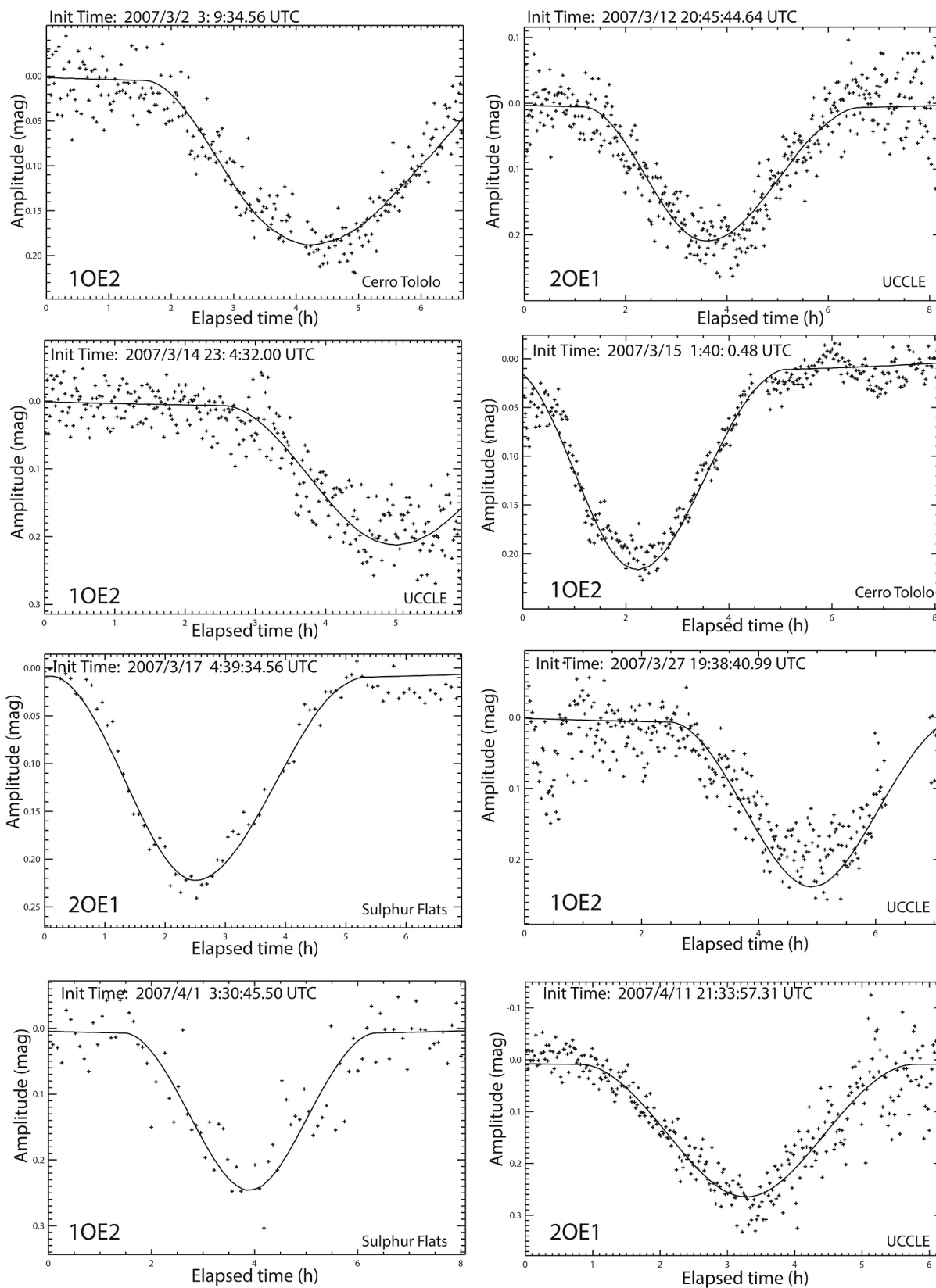


Fig. 2. Best collected light curves of 2007 Mutual events. The fitted solution is superimposed to the observations. Index 1 refers to Patroclus and index 2 to Menoetius. Type of event (Occultation or/an Eclipse) are given.

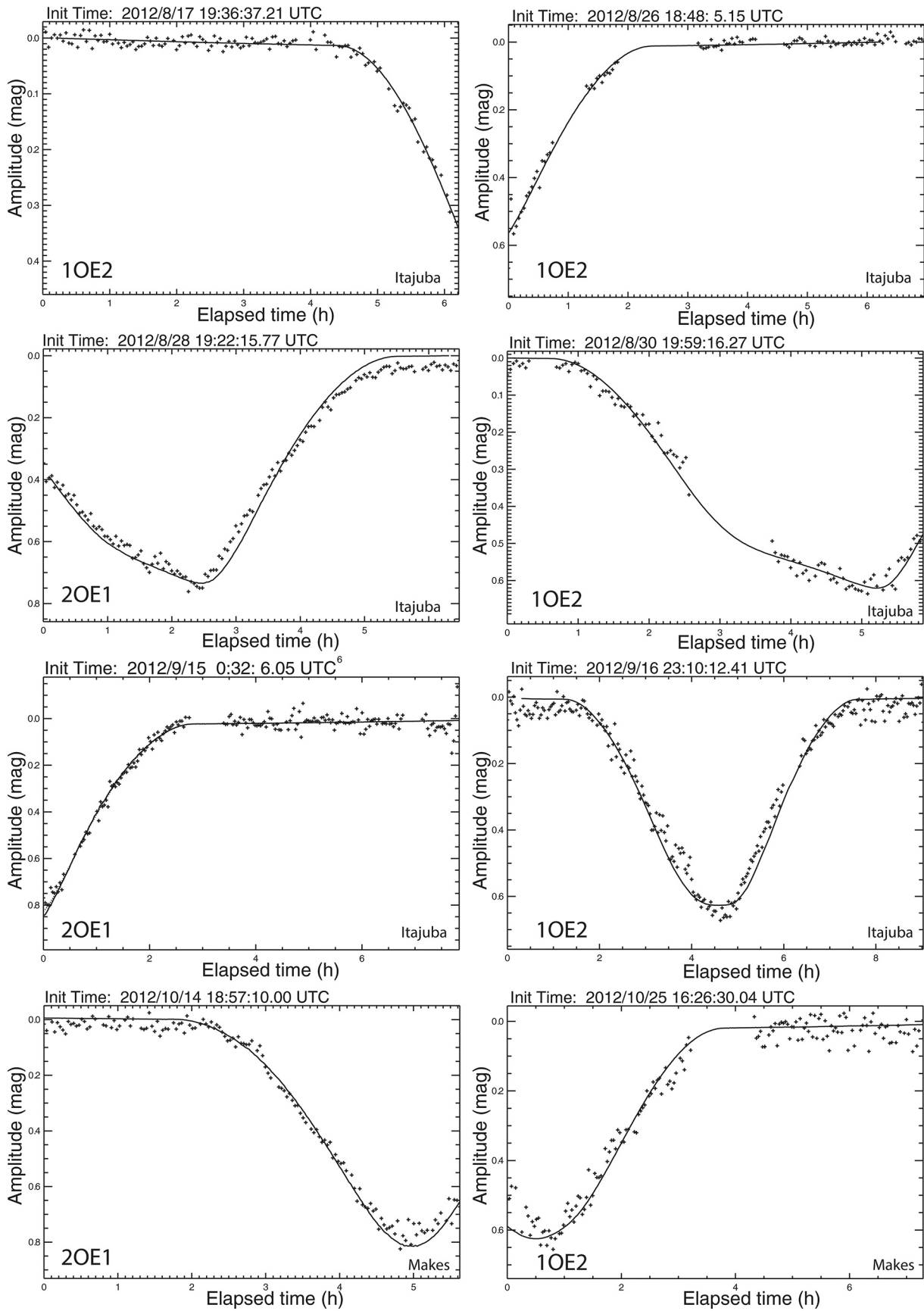


Fig. 3. Best collected light curves of 2012 Mutual events.

Table 2

List of observed times of minimum of light with the corresponding magnitude drop. The time interval elapsed since the first observation is given (Dt). The type of phenomenon indicates whether it is an occultation (O), an eclipse (E) or a combination of both (OE). Index 2 refers to the smallest component in diameter (Menoetius) and index 1 to the largest component (Patroclus). The orbital period is fitted so that between each observation there is either a whole number of revolutions or a whole number of half revolutions. We derived a preliminary value of the period $P = 102.79097 \pm 0.00037h = 4.282957 \pm 0.000015\text{days}$.

Date event	Type event	Time of minimum of light (UTC)	Magnitude drop	Phase (°)	Sub-Earth latitude (°)	N periods	Dt (days)
03/02/2007	1OE2	07:36.7 ± 2.8	0.19 ± 0.03	5.42	-6.25	0	0.0
03/13/2007	2OE1	00:31.6 ± 1.0	0.21 ± 0.03	4.01	-5.25	2.5	10.704815
03/15/2007	1OE2	03:46.5 ± 7.2	0.21 ± 0.03	3.74	-5.18	3.0	12.840394
03/17/2007	2OE1	07:02.1 ± 14.5	0.22 ± 0.03	3.49	-5.12	3.5	14.976007
03/28/2007	1OE2	00:42.1 ± 2.8	0.24 ± 0.03	2.69	-4.83	6.0	25.712092
04/01/2007	1OE2	07:22.7 ± 7.9	0.24 ± 0.03	2.70	-4.74	7.0	29.990278
04/12/2007	2OE1	00:51.9 ± 3.3	0.26 ± 0.03	3.54	-4.59	9.5	40.718727
08/28/2012	2OE1	21:23.8 ± 12.4	0.73 ± 0.03	7.28	-2.46	468.5	2006.574399
08/31/2012	1OE2	00:51.9 ± 17.4	0.62 ± 0.03	6.95	-2.55	469.0	2008.718891
09/17/2012	1OE2	03:43.8 ± 4.2	0.63 ± 0.03	4.70	-1.77	473.0	2025.838275
10/14/2012	2OE1	23:51.5 ± 2.6	0.82 ± 0.03	6.50	-1.86	479.5	2053.676968
10/25/2012	1OE2	17:08.7 ± 15.1	0.63 ± 0.03	8.21	-1.50	482.0	2064.397245

deduce the density of the grain at the surface.

The solution of the system is built in successive steps by determining the general parameters independently of each other. These parameters fall into two main groups. On the one hand the rotation parameters: orbital revolution period (Section 2) and pole position (Section 4). On the other hand, the parameters of the physical model adopted, i.e. a system made of synchronous heterogeneous equilibrium Roche ellipsoids (Section 3): the volume ratio (Section 4) the normalized angular velocity and the exponent of the internal density law (Section 5). This general model thus consists of a large set of parameters that are intimately intertwined with each other. The methodology adopted allows to decorrelate them from each other thanks to the collection of photometric observations made in 2007 and 2012 under different aspect and phase angles. The parameters are thus determined step by step, one after the other. This leads to a set of initial values of the parameters that are then refined in a new iteration to arrive at a coherent set capable of reproducing all the photometric observations. It should be kept in mind that in this model, the system is doubly synchronized in both rotation and revolution. Its dynamics is driven by Kepler's 3rd law assuming a purely circular orbit, which relates period and mutual separation to the size and shape of each component.

2. Observations

On the basis of the knowledge, in early 2007, of the dynamical and physical properties of Patroclus system (Marchis et al., 2006b), we organized an international campaign to maximize the coverage of observations of the 50 mutual events we predicted (Marchis et al., 2006d). To prepare this campaign, we also lead observations of Patroclus in 2004–2005 using the Keck 10-m-telescope Laser Guide Star Adaptive Optics system (Marchis et al., 2006a), and with the Infrared Spectrograph (IRS) on board of the Spitzer Space Telescope (Marchis et al., 2006c; Mueller et al., 2007, 2010). The first mutual events observed in January 2007 was successful (Marchis et al., 2007), suggesting a future rich harvest of data. Finally 10 observatories (listed in Table 1) have been a part of the campaign, and we gathered 35 light-curves, covering most of the full duration of the predicted mutual events.

In 2012, despite the data collected during the former campaigns, and all other adaptive optics and space observations at our disposal, the uncertainties about the parameters of the dynamic model of the Patroclus system did not allow us to have confidence in the prediction of the timings of the 2012 mutual events. We decided to organize a restricted campaign of observations, involving only our teammates and 3 observatories (see Table 1). From July to December 2012, we gathered 59 nights of photometric observations.

Some of the photometric observations carried out showed no phenomena or only a very small noisy portion of an event. This is why we extracted the best light curves that can really be exploited: 8 light curves

in 2007 (Fig. 2) and another set of 8 light curves in 2012 (Fig. 3).

3. Synodic period determination

So far the orbital revolution period has been accurately determined only from astrometric observations of the relative positions of Menoetius and Patroclus. Marchis et al. (2006b) reported a $4.283 \pm 0.004\text{days}$ period from an adaptive optics observation set collected in 2005 and 2006. Grundy et al. (2018), from an independent set of observations, performed on the HST, resulted in a value of $4.282680 \pm 0.000063\text{days}$ in the case of a circular orbit and $4.282696 \pm 0.000074\text{days}$ under a slightly elliptical orbit solution. On the other hand, the measurement of the period of revolution by analysis of the periodic variations of the light curve is made extremely difficult because of the very low amplitude photometric variations outside any period of mutual phenomena. Mueller et al. (2010) reported a period of $4.2925 \pm 0.0002\text{days}$ with an amplitude of $0.070 \pm 0.005\text{mag}$. Oey (2012), from photometric observations conducted in August 2011, obtained a compatible value within less than 2 sigma of $4.3125 \pm 0.0125\text{days}$ with an amplitude of $0.06 \pm 0.02\text{mag}$. We must emphasize that these last two determinations are based on photometric observations. Consequently the reported periods are synodic periods and not sidereal periods as is the case for determinations using astrometric observations by adaptive optics. As the motion around the sun is in the same sense as the direction of asteroid rotation, the synodic period is longer than the sidereal period. Purely as an indication, the difference between the two periods can be approximated by the relation [1], considering the Patroclus mean motion $n = 0.08277089^\circ / d$:

$$P_{syn} - P_{sid} = \frac{nP_{syn}^2}{360^\circ} = 0.00423d \quad (1)$$

The method used in this work is exclusively based on the measurement of the mid-eclipse times of light minima observed during the 2007 and 2012 mutual event seasons. However this direct method has its limitations. Indeed, strong phase effects and mutual shadowing (during eclipses) explain the fact that the times of the light minima are not separated from each other by a whole number of periods or half-periods of revolution. Firstly, we measured the mid-eclipse times by carrying out a fitting of the region near the minimum with a quadratic function. Table 2 lists the observed times of the mid-eclipse events.

For each event, we determine the number of periods n_i elapsed during a time interval Dt_i counted from the first recorded event. We assume a relationship of the form $Dt = A + P_{syn}n$ where P_{syn} is the unknown synodic period to be determined. We then proceed to the fit of the paired data (Dt_i, n_i) to the linear model. Table 2 gives the set of data (Dt_i, n_i) for each mid-event observed. We derived $A = 0.098 \pm 0.079h$ and $P_{syn} = 102.79097 \pm 0.00037h = 4.282957 \pm 0.000015\text{days}$. This initial value was then used together with a general model of the system

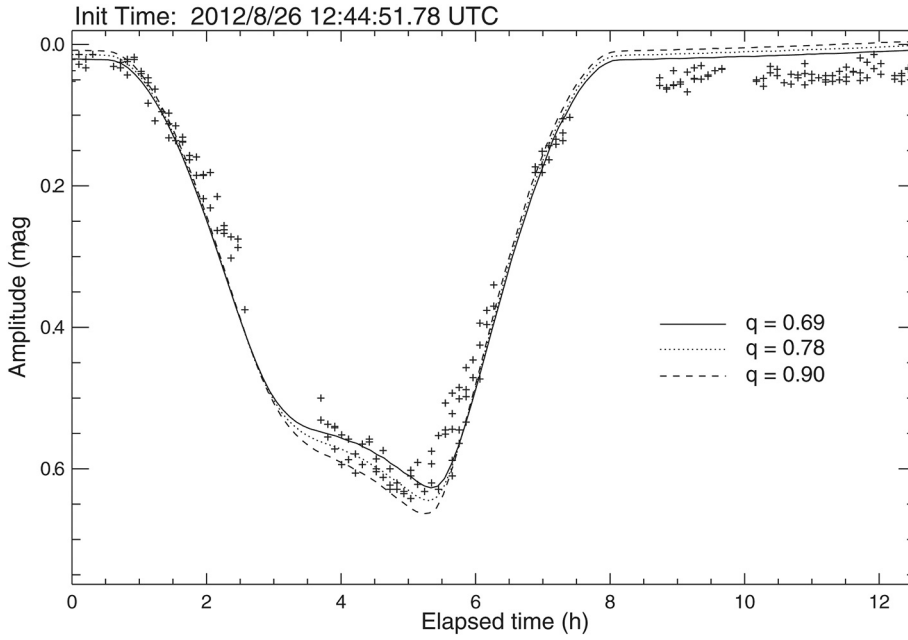


Fig. 4. Effect of the volume ratio on the shape and amplitude of the light curve. The light curve of 2012 was derived from the concatenation of observations of 26 and 30 August 2012. Geometry of the events are roughly identical (see Table 2) in such a way that the data of August 30 could thus be translated on those of August 26 thanks to the knowledge of the period of orbital revolution, thus making it possible to reproduce what could have been the complete light curve of the event of August 26.. The volume ratio only plays on the amplitude but by no means on the shape of the light curve. The value which minimizes the standard deviation is $q = 0.69 \pm 0.08$.

taking into account the phase angle photometric effects described in the following sections.

4. Physical model of the system

We applied a model of heterogeneous Roche equilibrium ellipsoids to the problem (Descamps, 2010) assuming the same bulk density for each component. In this model, the density distribution inside the body is described by a power law relation with radius. It was already successfully applied to small double asteroids such as Lundaia, Berna, Debussy and Tama. It allows at the same time to determine the bulk density and the grain density on the surface and thus the macroscopic porosity. The only parameter of this density law is the exponent n . In the case $n = 0$, we have a uniform mass distribution. From such a density law, we can infer a simple relation between the bulk density ρ_b and the grain density ρ_g of the constituent material:

$$\frac{\rho_b}{\rho_g} = \frac{3}{2n+3} \quad (2)$$

The main effect of the exponent is connected to the amplitude of the fundamental light curve. The greater the value of the exponent the greater the amplitude of the rotational light curve. We place ourselves in the general hypothesis of an identical bulk density for each of the two components of the system in such a way that the volume ratio is then equal to the mass ratio. Furthermore, it is reasonable to assume that the two components are largely identical in composition and therefore should have as well very similar albedos as it was already observed for a couple of binary systems (Laver et al., 2009; Marchis et al., 2011). For example, mutual events within the binary system Patroclus-Menoetius were used to derive thermo-physical properties of the surface of both objects (Mueller et al., 2010). The observations are consistent with identical surface regolith properties. Therefore, in the rest of the work, we have assumed identical surface properties and bulk densities of both components.

The general resolution of the problem depends on the normalized angular velocity Ω which is defined by

$$\Omega = \frac{\omega}{\sqrt{\frac{4}{3}\pi\rho_b G}} \quad (3)$$

A preliminary determination of Ω can be done by simple graphical

measurements of the light curve when the system is seen edge-on. The methodology is as follows. The duration of each event, ΔT , when the system is observed equatorially, depends mainly on two parameters: Ω and q , the volume ratio between the two components $q = (R_s/R_p)^3$ where R_p is the primary radius (Patroclus) and R_s the secondary radius (Menoetius). So far there are only two independent determinations of the volume ratio, one coming from AO observations (Marchis et al., 2006b), they found 0.79, and the other from the observation of a stellar occultation in 2013 (Buie et al., 2015), they found a value of 0.78.

Let P the orbital period, the relationship between the relative duration $\Delta T/P$ and the normalized angular velocity Ω can be readily derived from the equation for spherical bodies (Descamps et al., 2020):

$$\Omega = \sqrt{\pi^3 \frac{1+q}{(1+q^{1/3})^3} \left(\frac{\Delta T}{P}\right)^3} \quad (4)$$

To this end, we first considered the 2012 observation assuming in this first step that at this time the orbital plane is in the line-of-sight plane. The duration of the occultation event is straightforwardly inferred from the light curve itself. Only one complete phenomenon was observed, that of 16 September 2012 (Fig. 3). We measured $\Delta T = 6.34$ h (or $\Delta T/P = 0.062$). The normalized angular velocity is poorly sensitive to the value of the volume ratio, therefore without loss of generality we will admit a value of the volume ratio $q = 0.79$. This parameter will be redetermined subsequently in the section 4. Finally we get an initial value $\Omega = 0.043$ knowing that the exact value is necessarily lower because an event is always a combination of both an occultation with an eclipse owing to small phase angles that automatically increases the duration of the event. The final value will be determined accurately after obtaining the orbital pole solution (Section 4). The same applies to the exponent n (Section 5) which at first is supposed to be zero.

Once the normalized angular velocity of the system is known, the Roche equations give a unique solution in terms of shapes (triaxial ellipsoids) and sizes of the components and relative mutual separation. Each ellipsoid is represented by a 3D polyhedron made by a set of facets. Once the line of sight and the direction of Sun are known, it suffices to select the facets that are both visible by the observer and illuminated by the Sun. The total reflected light is then computed by adding the contribution of each of these active facets. The model incorporates a solar light scattering law as well as the photometric effects of mutual

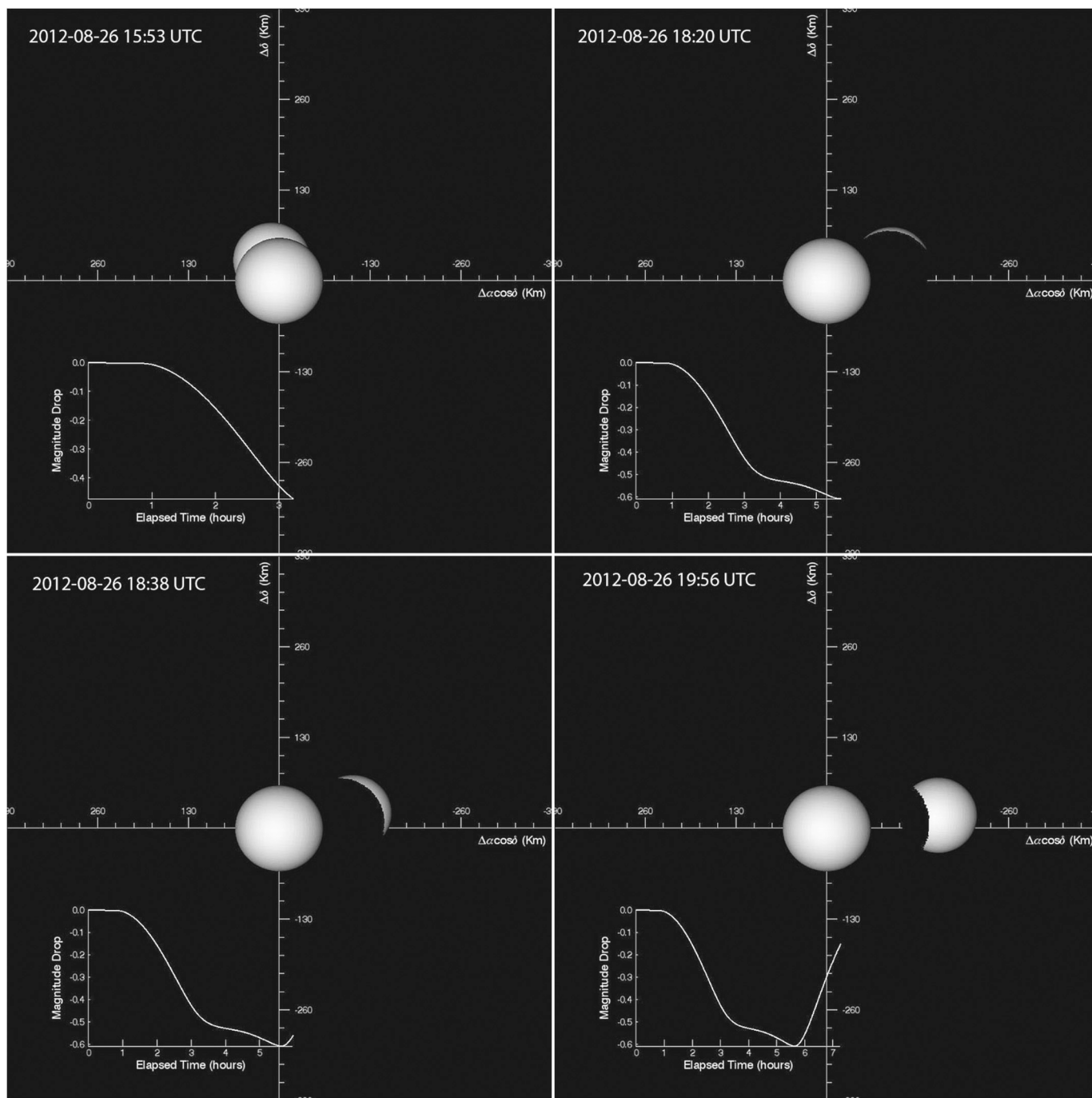


Fig. 5. Visualization of the course of the phenomenon of August 28, 2012 with the corresponding light curve. It is an occultation immediately followed by an eclipse of Menoetius by Patroclus. The effect of the significant phase angle (7.3°) generates an asymmetric, highly distorted light curve near the minimum of light where Menoetius is then almost completely immersed in the shadow cast by Patroclus. At this moment, the light comes from only one component of the system, Patroclus, the one with the largest diameter. The modelling of this observation is particularly sensitive to the ratio of the diameters as shown in Fig. 4. In this case, the magnitude drop observed for the minimum of light is related to the volume ratio by Eq. (2). The recorded magnitude drop is $0.62 \pm 0.02\text{mag}$, which implies a volume ratio $q = 0.69 \pm 0.08$.

shadowing between components. The same global photometric properties, e.g. albedo and scattering, have been assumed for both bodies. The adopted light scattering law is the single-parameter Minnaert law (Minnaert, 1941). The limb-darkening parameter was derived in Section 4.

5. Volume ratio and orbital pole

The position of the orbital pole and the size ratio between components, given by the value of the volume ratio, are strongly correlated parameters. Indeed, the magnitude drop or the shape of the photometric light curves depend significantly on them. However, it is possible to succeed in separating their effects in the photometric light curves, especially in the case of mutual phenomena observed at high phase

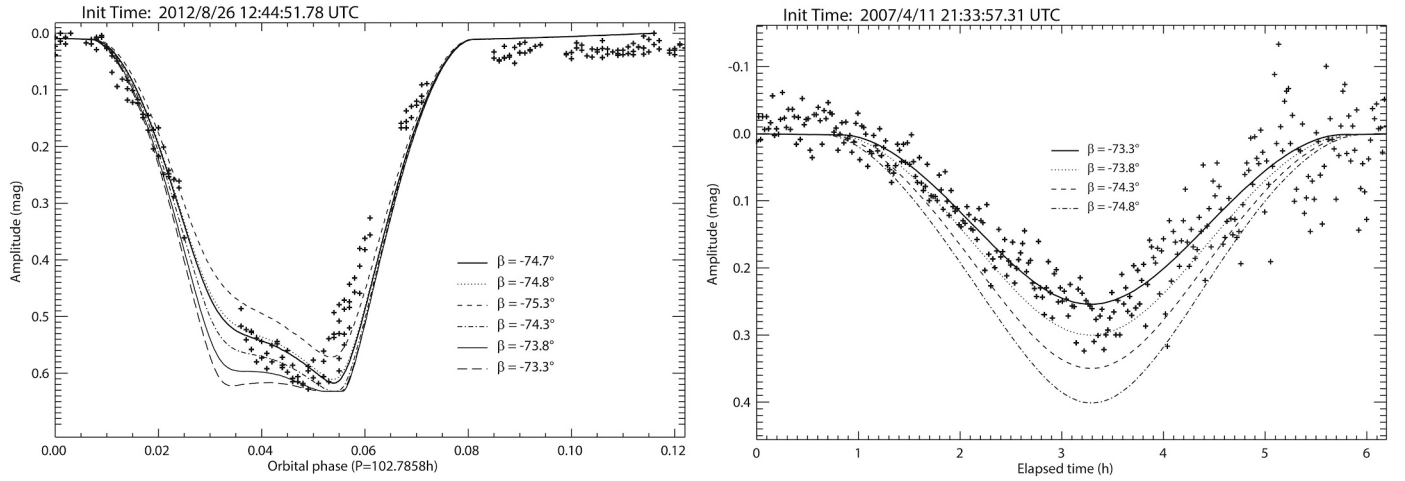


Fig. 6. The variation of light recorded in 2007 and 2012 is extremely sensitive to the value of the declination of the pole. Its general shape is deformed under the action of the variation of the declination of the rotation pole while keeping the value of the volume ratio equal to 0.69. A slight variation of only 1° is sufficient to cause a dramatic change in the amplitude of ~ 0.2 mag in the 2007 light curve.

angles, as was the case in the observation of August and September 2012. First of all, let us review our current knowledge of the orbital pole. [Marchis et al. \(2006b\)](#) reported an orbit pole located at the J2000 ecliptic longitude $\lambda = 236 \pm 5^\circ$ and latitude $\beta = -61 \pm 1^\circ$ which correspond to the equatorial coordinates $\alpha = 184 \pm 5^\circ$ and $\delta = -74 \pm 5^\circ$. [Grundy et al. \(2018\)](#) found $\lambda = 234.2 \pm 1.2^\circ$ and $\beta = -62.11 \pm 0.53^\circ$ ($\alpha = 179.3 \pm 1.8^\circ, \delta = -74.11 \pm 0.60^\circ$), this is the solution we adopted as our initial solution to study the volume ratio.

With such an orbital pole solution, it is straightforward to note that in 2012 the system was viewed nearly edge-on. The correlation between the position of the orbital pole and the volume ratio is then more effective. This can be seen in particular on the light curve of 28 August 2012 ([Figs. 4 and 6](#)). Nevertheless the photometric effects of each parameter are not strictly identical. Indeed, a variation in the declination of the pole causes in the region of the light minimum a deformation of the light curve which tends to approach a plateau ([Fig. 6](#)). Conversely, a variation in the volume ratio is equivalent to translating the light curve without really deforming it. Moreover, as shown in the visualization of the phenomenon ([Fig. 5](#)), which is an occultation immediately followed by an eclipse of Menoetius by Patroclus, such a shape of the light curve

can only be obtained by the complete immersion of Menoetius in the shadow cast by Patroclus. This effect is accentuated by the fact that the phase angle was then very significant (7.3°). At this moment, the light therefore comes from only one component of the system, Patroclus, the one with the largest diameter. The modelling of this observation is particularly sensitive to the ratio of the diameters as shown in [Fig. 4](#). In this case, the magnitude drop observed for the minimum of light is related to the volume ratio by the following equation:

$$\Delta mag_s = 2.5 \log \left(\frac{I_p + I_s}{I_s} \right) = 2.5 \log (1 + q^{2/3}) \quad (5)$$

With an observed magnitude drop of 0.62 ± 0.02 mag, we can infer a new value for the volume ratio: $q = 0.69 \pm 0.08$ (which gives a diameter ratio of 0.88 ± 0.04). From such a determination, the Minnaert limb darkening parameter best matching the overall lightcurves, and especially the differential magnitude of ~ 0.2 mag between the observed minimum of light in 2012 (see [Table 2](#)) including mutual shadowing effects, is $k = 0.9 \pm 0.1$.

[Table 2](#) shows that the recorded magnitude drops are much smaller in 2007 than in 2012. This means that the orbital plane of the double

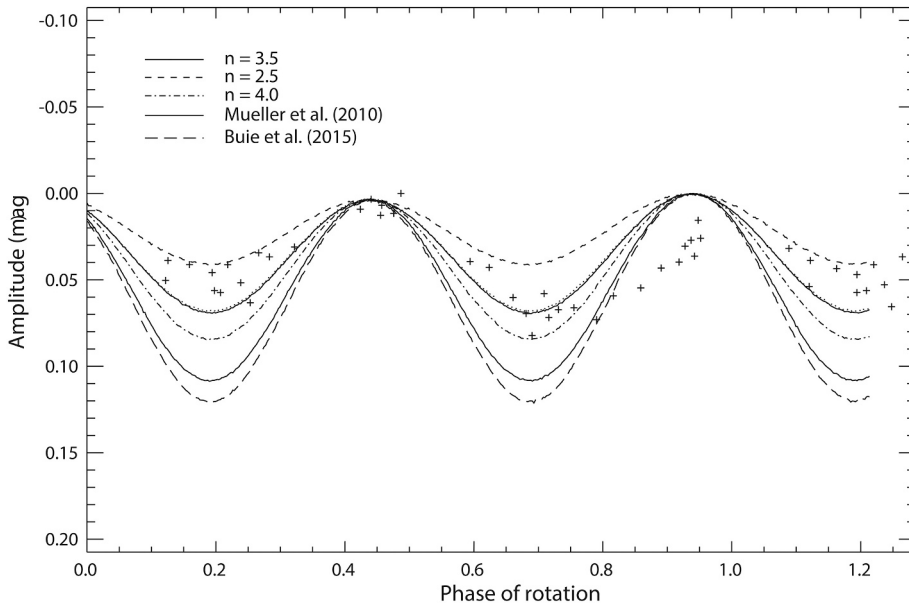


Fig. 7. Synthetic light curves derived from different models for the composite rotational light curve obtained in April 1996 and published in [Mueller et al. \(2010\)](#). The best solution is derived for our model with $n = 3.5 \pm 0.1$. The effect of the pole solution over the amplitude of the light curve is insignificant because at this time the system was widely opened over the line of sight. This type of observation is highly constraining for determining the parameter n . Light curves deriving from shape solutions given by [Mueller et al. \(2010\)](#) and [Buie et al. \(2015\)](#) are also superimposed. They clearly do not match the observations.

Table 3

Solutions of the inhomogeneous Roche problem. The bulk porosity includes the small-scale microporosity and the large-scale macroporosity (empty space). The primary and the secondary are described by their semi-axes (a_p, b_p, c_p) and (a_s, b_s, c_s). The relative separation D is defined as $(a_p + a_s)/d$, where d is the orbital separation of the system. Values of macroscopic physical parameters (grain densities and bulk porosities) are intrinsically connected with the adopted model of internal density distribution. Values are given with their 1-sigma error.

Synodic period (h)	Ω	q	n	ρ_b (g/cm ³)	ρ_g (g/cm ³)	p	b_p/a_p	c_p/a_p	b_s/a_s	c_s/a_s	D
102.786 ± 0.0004	0.036 ± 0.002	0.69 ± 0.08	3.5 ± 0.1	0.81 ± 0.16	2.69 ± 0.36	70 ± 10%	0.964 ± 0.008	0.938 ± 0.016	0.946 ± 0.008	0.921 ± 0.016	0.178 ± 0.008

Table 4

Relative astrometry in the plane of sky (X_{obs}, Y_{obs}) of Menoetius with respect to Patroclus from Roth et al. (2001), Marchis et al. (2006b) and Grundy et al. (2018). Relative positions from our solution (X_{calc}, Y_{calc}) are obtained for a minimum goodness-of-fit separation of 695 ± 10 km. Residuals in X and Y are reported.

Observation date (UTC)	X_{obs} (arcsec)	Y_{obs} (arcsec)	X_{calc} (arcsec)	Y_{calc} (arcsec)	$(O - C)_X$ (arcsec)	$(O - C)_Y$ (arcsec)
09/02/2001 14:42:34	-0.19800	-0.00680	-0.21974	-0.07098	+0.02174	+0.06418
10/13/2001 11:25:48	-0.07550	-0.09230	-0.08599	-0.10697	+0.01049	+0.01467
02/06/2002 06:13:09	-0.09900	-0.11000	-0.11000	-0.09110	-0.01733	-0.01890
02/07/2002 06:54:11	-0.15980	+0.01000	-0.17460	+0.01002	+0.01480	-0.00002
11/02/2004 15:29:51	0.01940	-0.05190	+0.01438	-0.05689	+0.00502	+0.00499
02/26/2005 09:46:06	-0.00750	-0.08250	-0.08287	-0.08953	-0.00463	+0.00703
03/01/2005 10:22:53	+0.18600	+0.05000	+0.17809	+0.04682	+0.00791	+0.00318
04/30/2005 06:56:21	+0.05230	+0.05230	+0.14223	+0.05386	-0.00033	-0.00156
05/28/2005 06:44:15	-0.14820	-0.03110	-0.14614	-0.03357	-0.00206	+0.00247
10/21/2013 06:43:00	-0.2463	-0.0185	-0.23835	-0.01303	-0.00795	-0.00547
05/20/2017 13:09:00	+0.1434	-0.0062	+0.13890	-0.00727	+0.00450	+0.00107
05/29/2017 22:44:00	-0.0194	-0.0585	-0.01628	-0.05880	-0.00312	+0.00030
06/08/2017 00:27:00	-0.1138	-0.0498	-0.11653	-0.04897	-0.00132	-0.00083
06/13/2017 12:21:00	-0.0646	+0.0356	-0.06735	+0.03702	+0.00275	-0.00142
06/14/2017 07:25:00	+0.0932	+0.0542	+0.09223	+0.05107	+0.00097	+0.00313
12/09/2017 14:36:00	-0.1443	+0.0102	-0.14078	+0.00873	-0.00352	+0.00147

system was then more inclined on the line of sight. A slight variation in the declination of the pole of rotation is then accompanied by large variations in the magnitude drop as it is shown in Fig. 6. With the value of the volume ratio previously determined, the best fitted pole solution from 2007 observation is $\alpha = 179.1 \pm 0.9^\circ$ and $\delta = -73.3 \pm 0.1^\circ$ ($\lambda = 232.6 \pm 1.2^\circ, \beta = -61.7 \pm 0.2^\circ$). While in 2012 we get $\alpha = 179.1 \pm 0.9^\circ$ and $\delta = -74.7 \pm 0.1^\circ$ ($\lambda = 235.3 \pm 1.2^\circ, \beta = -62.4 \pm 0.2^\circ$), solution which is compatible with the solution of Grundy et al. (2018). However, remarkably, we can note that the solution obtained from our 2012 observations is not compatible with that obtained from the 2007 observations. They deviate significantly from each other by a little more than one degree. Further observations of upcoming mutual events in 2024 will be valuable to settle definitely the pole solution.

6. Geometrical solution and sidereal period

Once the pole solution and the volume ratio have been obtained, it is then possible to determine the value of the exponent n using a composite light curve obtained from April 1996 observations and published by Mueller et al. (2010). At this time, the system was widely opened over the line of sight such that the effect of the pole solution over the amplitude of the light curve is then insignificant. The latitude of the sub-Earth point was $l_{sep} = -19.7 \pm 0.9^\circ$. In this configuration, the very small photometric variations in the light curve of the system result mainly from the elongation of the ellipsoids of revolution given by Roche's equations. Thus, it is possible to fit the last parameter of the physical model, the exponent n . To this end, several synthetic light curves are superimposed to the data in Fig. 7. The best solution derived from our model is obtained for $n = 3.5 \pm 0.1$. With such a model it only remains to fit the normalized angular velocity to each light curve collected in 2007 and 2012. The final resulting synthetic light curves are shown on the solid line in Figs. 2 and 3. The best-fit normalized angular velocity is $\Omega = 0.036 \pm 0.002$ and the corresponding physical and geometrical solution is given in Table 3. Our solution given compares to the models proposed by Mueller et al. (2010) who gives an ellipsoidal shape with

axial ratios 1.07:1:1, and by Buie et al. (2015) where the axis ratios are 1.3:1.21:1. Our shape model for the primary is 1.066:1.027:1 and for the secondary 1.086:1.027:1. Fig. 7 clearly shows that shape solutions derived by Mueller et al. (2010) and Buie et al. (2015) do not match the observations. Our ellipsoidal solutions for each component are much less oblate with very small flattening.

The value of the orbital period was ultimately refined. With our full model, it then makes it possible to determine precisely the instants of magnitude drop including all involved photometric effects. As our model is based on the rotation sidereal period of the system, the best fitted value is $P_{sid} = 102.78624 \pm 0.00015h = 4.282760 \pm 0.000005$ days able to match the observed times given in Table 2 with a standard deviation of 3 min which is equivalent to a precision on the relative positions of 2 km or 0.6 mas in 2012. We note that $P_{syn} - P_{sid} = 0.00473d$ to be compared with the theoretical value given by Eq. (1). Quite obviously, it is reminded that the underlying assumption is the perfect synchronization between rotation and revolution so that the system rotates like a solid body.

7. Mutual separation and physical dimensions of the shape models

So far dimensions and distances in our solution are only relative. The knowledge of the separation alone in kilometres immediately gives the physical dimensions of the ellipsoids according to Table 3. We used to this end the astrometric observations published by Marchis et al. (2006) and Grundy et al. (2018). They were made from Hubble Space Telescope and ground-based Keck telescope and are listed in Table 4. Additional observations taken in 2001 and 2002 with Hokupa'a mounted on Gemini North come from the Gemini Science archive (Roth et al., 2001). For each date we calculated the relative position of Menoetius with respect to Patroclus in the plane of sky. The best-fit separation d is derived by minimizing the dispersion of residuals. As our solution assumes a perfectly rigid rotation, the orbit is considered as a strictly circular Keplerian orbit. We obtain a separation $d = 695 \pm 10$ km which

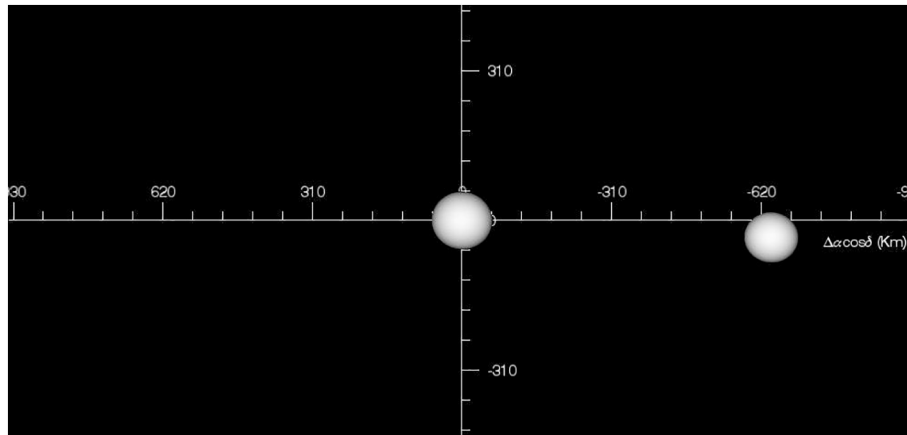


Fig. 8. Aspect of the system Patroclus-Menoetius for the 2013 October 21 stellar occultation.

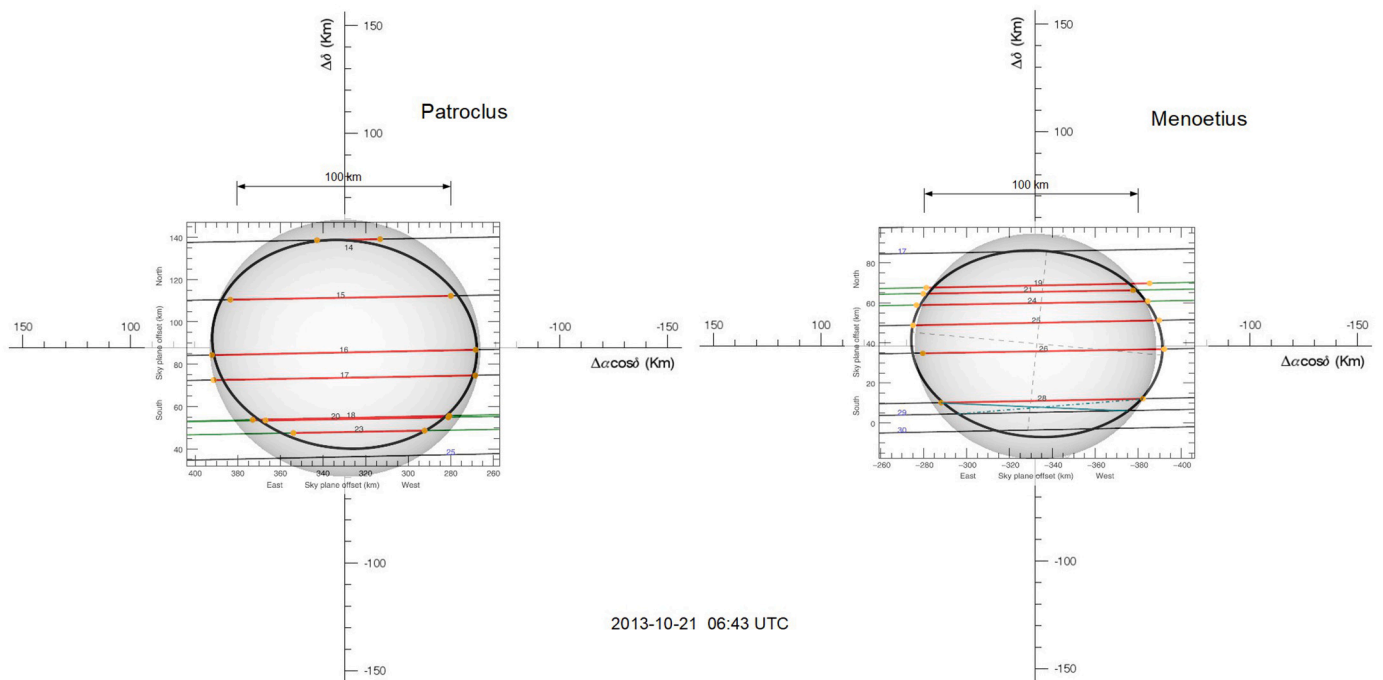


Fig. 9. : Stellar occultation by the Patroclus-Menoetius system on 2013 October 21. Figs. 5 and 6 of Buie et al. (2015) have been superimposed to the sky-plane projection of Patroclus (left) and Menoetius (right) derived from our solution (see text for explanations).

gives a resulting RMS of 9 mas in X and 16 mas in Y . Residuals drop respectively to 5,6 mas and 7,9 mas if only the 2004–2017 observations are considered. This value of the separation is consistent with the semi-major axis of $688.5 \pm 4.7\text{km}$ found by Grundy et al. (2018) from his set of observations.

Such a mutual separation yields a Patroclus ellipsoid of 130.8 by 126.2 by 122.8 km and a Menoetius ellipsoid of 117.1 by 110.8 by 107.8 km. The area-equivalent diameter of the system as a whole is defined by $D_A^2 = D_1^2 + D_2^2$. We derive $D_A = 168.8 \pm 2.6\text{km}$, in agreement with the value of Fernandez et al. (2003), $166.0 \pm 4.8\text{km}$, but significantly higher than the result of Mueller et al. (2010), $D_A = 145 \pm 15\text{km}$.

Buie et al. (2015) reported results of a stellar occultation by Patroclus and Menoetius on 2013 October 21 at 06:43:02 UTC. They deduced from these observations very oblate ellipsoidal shapes we saw earlier in Section 5 that they are not able to match the very small amplitude of the rotation light curve obtained by Mueller et al. (2010). If we apply our solution to this observation we obtain the relative positions given in Table 3 and the displayed position in Fig. 8 and 9. As the authors stated,

the earliest ingress time was 06:42:31.84 UTC and the latest egress time was 06:46:55 UTC. The chords were not obtained all at the same time, there is a motion along the orbit as the shadow crossed the network of stations. During this time interval, the quantitative change in relative position is $\Delta X = +0.7\text{km}$ and $\Delta Y = +1.39\text{km}$ which is negligible. No uncertainties on the relative positions are given by the authors. These positions are supposed to be the centers of the limb-fitted ellipses. Because of a less dense coverage of the observed chords in the Y direction, we can estimate this uncertainties at $\sim 2\text{km}$ in X and $\sim 5\text{km}$ in Y .

The apparent distance between Patroclus and Menoetius is then 642.2 km for a position angle of 266.9° , in rough agreement with the value given by the authors respectively 665.6 km and 265.7° , or a difference of 7.4 mas in apparent separation.

If we superimpose the profiles of Patroclus and Menoetius obtained from our solution to the chords plotted in Figs. 5 and 6 of Buie et al. (2015), we can note a good overall agreement on both the shape and size projected onto the sky plane, especially with regard to the length of the longest chords. However, the profile drawn by the chords deviates in

some places from the equilibrium ellipsoidal model. This deviation is of the order of 5 km but can go up to 10-15 km which may be due to the presence of large and deep craters. We should note, however, that chords #29 and #30 for Menoetius appear to be doubtful according to the authors. Further observations of stellar occultations are required.

8. Discussion

From our sidereal period determination, Eq. (3) gives a bulk density of $0.81 \pm 0.16 \text{ g/cm}^3$. It is in agreement with previous determinations of $0.8_{-0.2}^{+0.2} \text{ g/cm}^3$ from adaptive optics observations (Marchis et al., 2006) and 0.88 g/cm^3 (without error bars) from a stellar occultation (Buie et al., 2015). Mueller et al. (2010) found a slightly higher value of $1.08 \pm 0.33 \text{ g/cm}^3$ from thermal infrared observations.

With $n = 3.5 \pm 0.1$, we derive from Eq. (2) a grain density of $2.69 \pm 0.36 \text{ g/cm}^3$ and a resulting total (bulk & grain) porosity of $70 \pm 10\%$. This grain density is very close to the primitive CM carbonaceous chondrites (density of $\sim 2.71 \text{ g/cm}^3$ and a high average porosity of 12% characterized by significant water content analogues (Britt et al., 2002). More generally it ranges in the densities of the carbonaceous chondrites analogues - density of $\sim 2.42\text{--}5.66 \text{ g/cm}^3$ with an average of 3.44 g/cm^3 - with porosities ranging from 0 to 41% with an average of 17% (Macke et al., 2011). It is compatible with results from Near-infrared spectroscopy (NIR, $0.7\text{--}2.5 \mu\text{m}$) which has been used to characterize the population properties of Trojan surfaces (Emery et al., 2011). Two distinct spectral groups align with D- and P-type asteroid taxonomies. Notably, Patroclus is a member of the “less-red” group. The less-red group straddles the boundary between C-type and P-type. Hiroi et al. (2004) successfully reproduced visible NIR reflectance spectra of the P-type asteroids in terms of CI, CM and Tagish Lake meteorite samples. On the other hand, the mid-infrared emissivity spectrum of Patroclus (Mueller et al., 2010) has a weaker $10 \mu\text{m}$ feature that is a closer match to those of C-type asteroids. Our result on surface grain density, although derived from a theoretical model of hydrostatic equilibrium figures for an inhomogeneous interior, is consistent with the spectroscopic observations performed in NIR over the last decade. It could suggest a high bulk density of $\sim 50\%$ typical of loosely consolidated piles of collisional with a significant fraction of ice in its interior.

In this paper we have presented new results on key parameters of the Patroclus binary system (orbital pole, synodic orbital period, volume ratio, shape, density). For the first time, they were obtained from photometric observations alone of mutual phenomena between the two components of the system. The next such campaign will take place in 2024. This will be the last opportunity to constrain these parameters before the *Lucy* flyby of Patroclus. As shown in Fig. 1, the season will be particularly favourable since it will give rise to a close opposition on September 28, 2024 (distance of 3.52 au with a V magnitude of 14.57) in the very heart of a period of deep phenomena during which the system will be seen nearly edge-on. The southern hemisphere observatories will then be in the best position to observe these phenomena.

Declaration of Competing Interest

F.B-R acknowledges the CNPq grants 309578/2017-5 and Coordenação de Aperfeiçoamento de Pessoal de Nível Superior - Brasil (CAPES) - Finance Code 001. Part of the results is based on observations taken at Pico dos Dias Observatory of the National Laboratory of Astrophysics (LNA/Brazil).

References

- Berthier, J., Marchis, F., Descamps, P., Assafin, M., Bouley, S., Colas, F., Dubos, G., Emery, J.P., De Cat, P., Farrell, J.A., Leroy, A., Pauwels, T., Pollock, J.T., Reddy, V., Sada, P.V., Vingerhoets, P., Vachier, F., Vieira-Martins, R., Wong, M.H., Reichard, D. E., 2007. An observing campaign of the mutual events within (617) Patroclus-Menoetius binary Trojan system. American astronomical society, DPS meeting #39, id.35.05. Bull. Am. Astron. Soc. 39, 482.
- Britt, D.T., Yeomans, D., Housen, K., Consolmagno, G.J., 2002. Asteroid density, porosity and structure. In: Bottke, W.F., Cellino, A., Paolichci, P., Binzel, R. (Eds.), Asteroids III. University of Arizona Press, Tucson, pp. 103–112.
- Buie, M.W., Olkin, C.B., Merline, W.J., Walsh, K.J., Levison, H.F., Timerson, B., Herald, D., Owen Jr., W.M., Abramson, H.B., Abramson, K.J., Brett, D.C., Caton, D. B., Conard, S.J., Croom, M.A., Dunford, R.W., Dunford, J.A., Dunham, D.W., Ellington, C.K., Liu, Y., Maley, P.D., Olsen, A.M., Preston, S., Royer, R., Scheck, A.E., Sherrod, C., Sherrod, L., Swift, T., Taylor III, L.W., Venable, Roger, 2015. Size ad shape from stellar occultation observations of the double Jupiter Trojan Patroclus and Menoetius. Astron. J. 149, 113.
- Descamps, P., 2010. Equilibrium figures of inhomogeneous synchronous binary asteroids. Icarus 207, 758–768.
- Descamps, P., Vachier, F., Berthier, J., Normand, J., Wiggins, P., de Groot, H., Coudert, J., Chojnacki, V., Labrevoir, O., Joly, S., Marcon, J.-P., Olimpiade, S., Dargoui-Pister, B., Delhaume, C., Duval, T., El Farissi, Y., Giraud, M., Grieco, V., Kaderi, S., Laidi, A., Lauze, T., Mary, H., Medour, M., Negre, F., Passabet, K., Perret, A., Peyron, M., Ramos, N., Soridi, M., 2020. Physical characteristics of double asteroid (3905) Doppler. Icarus 345 article id. 113726.
- Emery, J.P., Burr, D.M., Cruikshank, D.P., 2011. Near-infrared spectroscopy of Trojan asteroids: evidence for two compositional groups. Astron. J. 141, 25.
- Fernandez, Y.R., Sheppard, S.S., Jewitt, D.C., 2003. The albedo distribution of jovian Trojan asteroids. Astron. J. 126, 1563–1574.
- Grundy, W.M., Noll, K.S., Buie, M.W., Levison, H.F., 2018. The upcoming mutual event season for the Patroclus-Menoetius Trojan binary. Icarus 305, 198–202.
- Hiroi, T., Pieters, C.M., Rutherford, M.J., Zolensky, M.E., Sasaki, S., Ueda, Y., Myamoto, M., 2004. What are the P-type Asteroids Made of? Lunar and Planetary Science XXXV.
- Laver, C., de Pater, I., Marchis, F., Adamkovic, M., Wong, M.H., 2009. Component-resolved near-infrared spectra of the (22) Kalliope system. Icarus 204, 574–579.
- Levison, H.F., Lucy Science Team, 2016. LPI 37, 2061.
- Macke, R.J., Consolmagno, G.J., Britt, D.T., 2011. Density, porosity, and magnetic susceptibility of carbonaceous chondrites. Meteorit. Planet. Sci. 46, 1842–1862.
- Marchis, F., Berthier, J., Hestroffer, D., Descamps, P., Merline, W.-J., 2006a. (617) Patroclus, International Astronomical Union Circular, 8666, p. 1.
- Marchis, F., Hestroffer, D., Descamps, P., Berthier, J., Bouchez, A.H., Campbell, R.D., Chin, J.C.Y., van Dam, M.A., Hartman, S.K., Johansson, E.M., Lafon, R.E., Le Mignant, D., de Pater, Imke, Stomski, P.J., Summers, D.M., Vachier, F., Wizinovich, P.L., Wong, M.H., 2006b. A low density of 0.8 g/cm^3 for the Trojan binary asteroid 617 Patroclus. Nature 439, 565–567.
- Marchis, F., Berthier, J., Descamps, P., Emery, J., Harris, A., Hestroffer, D., Mottola, S., Mueller, M., Vachier, F., 2006c. Eclipses and occultations on binary Trojan asteroid (617) Patroclus. Spitzer Prop. 30235.
- Marchis, F., Wong, M.-H., Descamps, P., Berthier, J., Hestroffer, D., Vachier, F., 2006d. (617) Patroclus, Central Bureau Electronic Telegrams, 533, p. 1.
- Marchis, F., Baek, M., Berthier, J., Descamps, P., Hestroffer, D., Vachier, F., Colas, F., Lecacheux, J., Reddy, V., Pino, F., 2007. (617) Patroclus, Central Bureau Electronic Telegrams, 836, 1.
- Marchis, F., Enriquez, J.E., Emery, J.P., Berthier, J., Descamps, P., Vachier, F., 2011. The origin of 90 Antiope from component-resolved near-infrared spectroscopy. Icarus 213, 252–264.
- Merline, W.J., Close, L.M., Siegler, N., Potter, D., Chapman, C.R., Dumas, C., Ménard, F., Slater, D., Baker, A.C., Edmunds, M.G., Mathlin, G., Guyon, O., Roth, K., 2001. In: Green, D.W.E. (Ed.), S/2001 (617) 1. IAU Circ., No. 7741, #2, 2001.
- Minnaert, M., 1941. The reciprocity principle in lunar photometry. Astrophys. J. 93, 403–410.
- Mueller, M., Marchis, F., Emery, J.P., Berthier, J., Hestroffer, D., Harris, A., Descamps, P., Vachier, F., Mottola, S., 2007. Spitzer observations of mutual events in the binary system (617) Patroclus-Menoetius. AAS/division for planetary sciences meeting abstracts #39 16.02.
- Mueller, M., Marchis, F., Emery, J.P., Harris, A.W., Mottola, S., Hestroffer, D., Berthier, J., di Martino, Mario, 2010. Eclipsing binary Trojan asteroid Patroclus: thermal inertia from Spitzer observations. Icarus 205, 505–515.
- Oey, J., 2012. The Minor Planet Bulletin, 39, pp. 106–107.
- Roth, K.C., Guyon, O., Chun, M., Jensen, J.B., Jorgensen, I., Rigaut, F., Walther, D.M., 2001. Hojupa'a performance and point spread function characterization. Bull. Am. Astron. Soc. 33, 785.
- Wong, I., Brown, M.E., 2019. Multiband photometry of a Patroclus-Menoetius mutual-event: constraints on surface heterogeneity. Astron. J. 157, 203.